ADVANCED INTELLIGENT SYSTEMS
Open Access
www.advintellsyst.com

Real-Time Force Monitoring of Electrically Stimulated 3D-Bioengineered Muscle Bioactuators Using Organic Sensors with Tunable Sensitivity

Stefano Lai, Judith Fuentes, Maria Guix,* Giulia Casula, Piero Cosseddu, and Samuel Sánchez**

The contractile nature of skeletal muscle tissue makes it especially attractive for powering biohybrid actuators. Significant efforts have been dedicated to the improvement and control of contraction force, going one step forward toward the automation of these biohybrid platforms. Herein, 3D-bioengineered skeletal muscle tissues are integrated with organic transistor-based sensors to define a soft bioactuator with real-time force monitoring capabilities. The muscle tissue is electrically stimulated while the organic sensor ensures transduction of the exerted force into an electrical signal that allows direct monitoring of the bioactuator performance. Sensor calibration is carried out to define its sensitivity at different biasing conditions: as opposed to standard, two-terminal piezoresistive devices, transistor-based strain sensors show tunable sensitivity by acting on the voltage applied to a third terminal—the gate. A complete evaluation of sensing performances is provided, demonstrating that real-time monitoring is effective under different conditions, including stimulation signal frequency and chemical modulation of the bioactuator contraction, demonstrating its potential use as a drug testing platform. In the reported results, the way is paved for a complete exploitation of organic devices in soft robotic applications and to the development of novel biohybrid machines in bioengineering and biomedicine.

1. Introduction

Small-scale actuators have made significant progress in healthcare and environmental applications, being of special interest toward precision medicine.[1,2] For controlled navigation of such robotic platforms, the integration of sensing elements that provide real-time information is required to realize precise tasks in a programmable manner. The integration of biological entities into robotic systems gave rise to the biohybrid robotics field, providing unique functionalities such as adaptability or self-healing.[3,4] The use of living materials in robotic systems has opened up a myriad of opportunities to incorporate properties that are particularly challenging to obtain in their synthetic counterparts. Particularly, the main challenges to tissue-engineered biohybrid robots involve implementing the best fabrication techniques for achieving optimal designs, accounting both for cell survival, efficient motion, and how to implement proper control mechanism toward its later automation.

In fact, the common configurations and control mechanics applied in conventional robotics cannot be directly implemented to biohybrid robots, as other constraints arise, such ensuring cell survival throughout the desired biorobot lifetime. Additionally, cell organization must be maintained, posing a clear challenge on the number and scale range of the robotic control components design. Formally, a robot is a machine that is controlled by a computer and can perform complex tasks automatically, meaning that such tasks are programmed beforehand. Indeed, when designing a robot is necessary to account for the workflow for automatic control of microrobots (*actuation—feedback—control—planning*).[5] The control mechanisms explored to actuate living robotics include electrical, optical, chemical, and magnetic control, and in some cases, combining/applying more than one

S. Lai, G. Casula, P. Cosseddu
Department of Electrical and Electronic Engineering
University of Cagliari
Piazza d'Armi, 09123 Cagliari, Italy
E-mail: stefano.lai@unica.it

The ORCID identification number(s) for the author(s) of this article can be found under https://doi.org/10.1002/aisy.202400407.

DOI: 10.1002/aisy.202400407

J. Fuentes, M. Guix, S. Sánchez
Institute for Bioengineering of Catalonia (IBEC)
Barcelona Institute of Science and Technology (BIST)
Baldiri-Reixac 10-12, 08028 Barcelona, Spain
E-mail: maria.guix@ub.edu; ssanchez@ibecbarcelona.eu

M. Guix
Department of Materials Science and Physical Chemistry, Institute of Theoretical and Computational Chemistry
University of Barcelona
08028 Barcelona, Catalonia, Spain

S. Sánchez
Institució Catalana de Recerca i Estudis Avançats (ICREA)
Passeig de Lluís Companys 23, 08010 Barcelona, Spain

mechanism. It should be noted that the most desirable mechanism for spatiotemporal control of untethered bioactuators is optical stimulation.[6,7] While directional control was achieved by a differential stimulation along the biohybrid robot body,[8] more advanced systems had been reported by integrating wireless passive optoelectronic devices that allow wireless control over its trajectory.[9] However, the requirement for optical stimulation demands genetic modification of the muscles cells to express light-sensitive proteins called opsins, increasing both the complexity of bioactuator fabrication and reducing the versatility and the force of the resulting actuator. Toward future biomedical applications, electrically stimulated robots would be more desirable for providing higher force, as a higher number of muscle fibers are activated under electrical stimulation compared to light stimulation.[10] Recently, a bipedal skeletal muscle robot demonstrated fine-tuned turning motions when selectively stimulating one of its legs by electrical pulses, achieving forward and stop motions.[11]

Apart from achieving a controlled spatiotemporal actuation, it is important to withdraw real-time information over the force exerted by the muscle, being the robotic element that provides for actuation in such biohybrid designs. Additionally, the evaluation of the contraction force of skeletal muscle tissues provides information about the level of cell maturation and functionality, key features in drug screening platforms when studying the effects of biomaterials, media components or drugs on muscle development and disease modeling.[12] Current efforts are devoted to integrating force measurement systems to obtain real-time information over the skeletal muscle tissue performance. For example, through evaluation of matrix deformation during contraction,[13] the use of cantilever-based system optical sensing,[14] magnetic sensing, and strain sensors.[15] A novel approach based on microscale compliant strain sensors coupled to 3D tissues demonstrated precise electrical sensing of mechanical responses under optical and chemical stimulation of optogenetically modified engineered muscle constructs actuated by light.[16] In our work, we propose the integration of a flexible strain sensor to an electrically stimulated muscle actuator to obtain real-time information over the force exerted by the 3D-engineered muscle. Flexible organic electronics represents a valuable technology for the development of different kinds of sensors that find application in the field of bioelectronics.[12–15] Organic materials are easily processed at room temperature, thus making possible the development of electronic devices on flexible and lightweight substrates. This characteristic allowed the application of organic electronic devices as sensors for mechanical deformation. In particular, the employment of organic field-effect transistors (OFETs) for strain sensing has been explored.[16–19] With respect to conventional, two-terminal piezoresistive strain gauges, in which the sensitivity is fixed by the geometry and the selection of materials, OFET-based strain sensors employ a third terminal, namely the gate, which allows modulation of the conductivity of the organic semiconductor and thus the sensing performance. Therefore, we are here proposing for the first time a programmable and complete electronic stimulation-feedback approach for monitoring biohybrid cell actuators.

The proposed organic transistor-based strain sensor configuration stands out for its high sensitivity, allowing different sensing modulation depending on the sensor deformation, and the possibility to decouple the signal of the recorded force from the electrical stimulation applied to induce the muscle contraction. Moreover, the unique mechanical and biocompatibility characteristics of organic materials make them more suitable for effective integration in soft robotics applications.[17,18] To ensure the optimal coupling of the muscle to the sensor, curved notches were additionally included not to impact on the muscle integrity during its actuation. By studying the muscle response to different stimulant and relaxant drugs, we demonstrated the feasibility of using such sensors in nongenetically modified muscle bioactuators, using controlled electrical pulses. Therefore, such sensing platforms are not only of interest for providing key information about the biological actuator, going one step toward their automation, but also for incorporation into other bioengineered muscle platforms due to their versatility and easy integration.

2. Results and Discussion

The design hereby presented considers not only the easy integration of the 3D skeletal muscle bioactuator, but also its viability during the whole sensing process. To do so, we integrated two polydimethylsiloxane (PDMS) notches by directly 3D printing them on the flexible electrodes. Situated at each end, and presenting similar widths to the flexible sensor, these notches ensure homogeneous deformation of the strain sensor during muscle contraction. Additionally, to keep the muscle in place they form a 1) curve path that allows easy integration the 3D-bioengineered muscle, also avoiding any side damage during the stimulation process and 2) a curved side view that prevent its release during the contraction–relaxation cycle. The assembly of the OFET-based strain sensor with the 3D-bioengineered skeletal muscle tissue is shown in **Figure 1**A. Details about the fabrication of sensors of the preparation of muscle tissues and of their integration on sensors are reported in Section 4. To perform experiments, the sensor area is immersed in the culture media with the electrodes for stimulation, and the muscle tissue is transposed on supports (pillars) 3D printed on the sensor surface (Figure 1B and Movie S1, Supporting Information). The muscle tissue contraction induced by the electrical stimulus imposes a force on the pillars, thus producing a bending on the sensor area. Thanks to the polycrystalline morphology of organic semiconductor, the surface strain induced by bending influences the charge carrier mobility: crystalline domains are brought close together by the compressive deformation, thus making charge carrier transfer along the film easier.[19–21] Consequently, the transistor output current I_{DS} changes, proportionally to the applied strain. Such current variations can be read by a front-end electronic circuit to be converted into voltage variations and thus available for analog-to-digital conversion and acquisition. Therefore, a real-time visualization of deformation is obtained: the larger the voltage signal variation, the larger the deformation applied by the muscle tissue to the transistor (Figure 1C).

2.1. Sensor Calibration

To link the recorded voltage variation with the deformation applied by the muscle, the sensors were preliminary calibrated

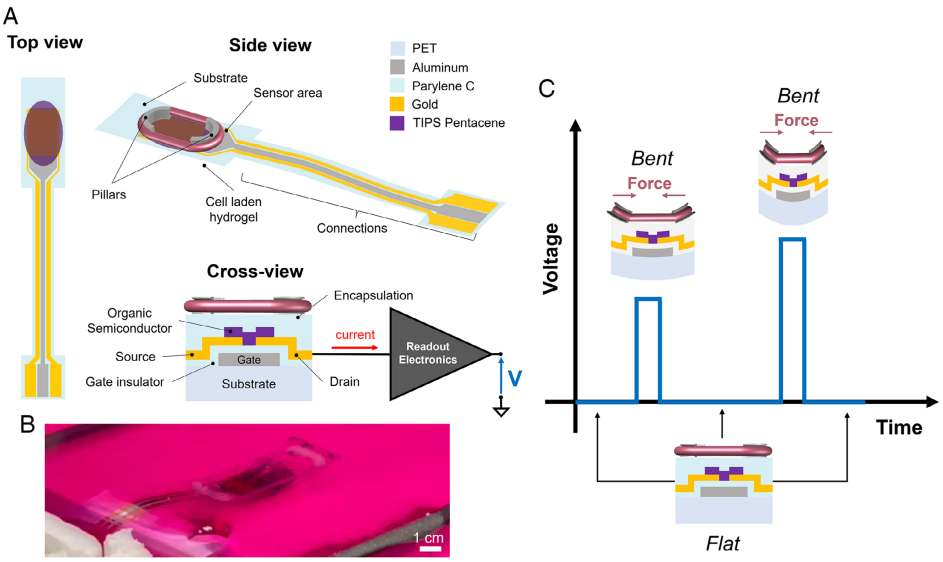

Figure 1. Schematic of the flexible organic sensor with integrated muscle bioactuator. A) Sensor structure in a top, side, and cross view. Details about structure and materials employed are shown on the latter. B) Picture of the muscle bioactuator assembled in PDMS-based notches on top of the sensor, all set up in a dish with culture media. C) Working principle of the device: when muscle tissue contracts, the sensor is bent, and the output voltage of the readout electronics changes proportionally to the applied strain.

in laboratory by means of a dynamometric system to precisely correlate the output signal (drain current variation) with applied forces. Results are reported in **Figure 2**. Figure 2A displays normalized transfer characteristic curves of a representative device, i.e., the current flowing between source and drain of the transistor as a function of the gate-to-source voltage (V_{GS}) and for a constant value of the drain-to-source voltage (V_{DS}). Each plot was obtained during the application of a given deformation related to a precise force applied by a mechanical indenter and controlled with a dynamometer (Figure 2C, details are reported in Section 4). Normalized current is $\Delta I_{DS} = I_{DS} - I_{DS,0}$, with I_{DS} being the transfer characteristic curve acquired during the application of a specific force value, and $I_{DS,0}$ being the transfer characteristic curve recorded while the device is flat (no force applied). It is possible to observe that the higher the force (i.e., the larger the deformation), the higher the transistor current, which is coherent with the application of a compressive strain to the organic semiconductor film. Another aspect to be highlighted is that the device response changes with the applied V_{GS} value. For V_{GS} values larger than 0 V, the device is in its subthreshold regime, so the applied deformation only slightly modifies the current. The more the voltage is driven negative, the more the transistor moves to its conductive state, allowing a larger current to flow in the channel. Consequently, a larger sensitivity to strain is obtained, as denoted by the increasing separation between plots related to different forces. This characteristic is better displayed by plotting ΔI_{DS} versus applied force for given V_{GS} values (Figure 2B): in this way, it is possible to observe that, for $V_{GS} \leq -1$ V, the device is still near to its off state, and so the current variation with applied force is not significant. The more the device enters in its on state, the more the current variation with force becomes significant. Figure 2B shows the calibration curves obtained at different V_{GS} values: by properly choosing a force range representative for the one that would

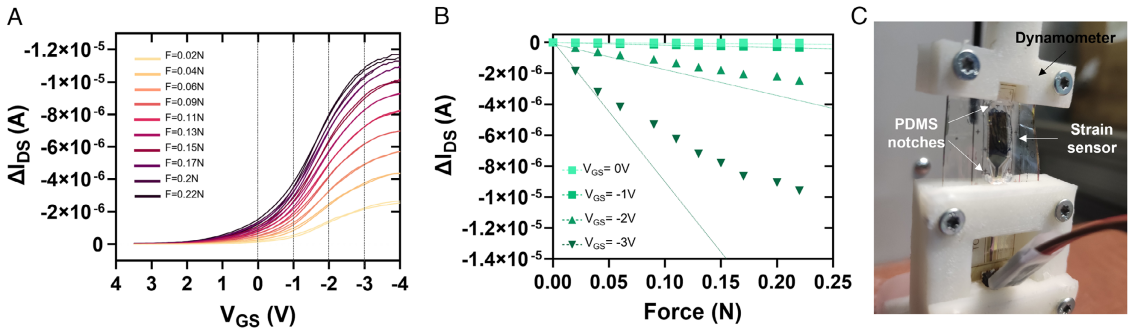

Figure 2. Calibration of the strain sensor. A) Normalized transfer characteristic curves $\Delta I_{DS} = I_{DS} - I_{DS,0}$ versus V_{GS}, evaluated at $V_{DS} = -5$ V and for different force values applied by the dynamometer. In the latter, I_{DS} is the transfer characteristic at a certain force value, while $I_{DS,0}$ is the transfer characteristic acquired for a device in the flat state ($F = 0$ N). B) Calibration curves obtained by plot (A) at fixed V_{GS} values (0, −1, −2, and −3 V). C) A detail of the 3D-printed measurement setup employed for calibration.

be transduced during application, the sensitivity of the sensor can be derived as the slope of the linear fitting. Average sensitivity performances of 22 sensors at different operating voltages are reported in Table S1, Supporting Information.

2.2. Assessment of Sensor Readout in Experimental Scenario

The evaluation of the sensor functionality for a correct force transduction of electrically stimulated muscle cells requires that several aspects are thoroughly examined. Since the sensor is directly exposed to the media where voltage pulses are applied to stimulate cell contraction, it is important to preliminarily demonstrate the absence of significant cross talk between stimulation and readout. Results of this preliminary test are reported in **Figure 3**, which also show the measurement setup (Figure 3E), composed of a petri dish containing culture media and modified with carbon electrodes for stimulation, the custom-made printed circuit board (PCB) for sensor readout and stimulator connection, and the digital control module used for data collection and visualization. The readout electronics convert the current variation of the transistor into a voltage, which is further conditioned to be effectively acquired by the digital control module and sent to a computer for data visualization. Details about front-end design and simulation are provided in Supporting Information.

First, sensors were characterized during the application of the voltage stimulus, but before the addition of the muscle bioactuator the printed support (Figure 3Ea). The stimulus employed was a monophasic voltage pulse train with an amplitude of 30 V, a duration of 2 ms, and a repetition frequency of 1 Hz; the sensor was biased at $V_{DS} = -5$ V and $V_{GS} = -3$ V to let it operate at maximum sensitivity. It is possible to observe that the system recorded only white noise at a maximum amplitude of about 10 mV, thus proving that the sensor response is not affected by the pulse applied in the culture media. By repeating the experiment in the same conditions on the same sensor after the application of the muscle cell actuator (Figure 3Eb), the sensor readout showed the presence of voltage peaks, well distinguishable from the noise band and clearly correlated to the evoked contraction of the muscle tissue. Moreover, the sensor demonstrated the capability of following contractions obtained at different repetition frequency of stimuli (2 and 5 Hz, Figure 3Ec,d, respectively).

2.3. Programmability of Sensor Sensitivity

A transistor-based mechanical sensor enables the capability of finely tune the sensitivity by modulating the gate voltage, thus providing a further degree of freedom to the feedback system. Indeed, the sensitivity can be adapted to the force range provided by the muscle tissue during operation, thus ensuring optimal sensing performances. It is noteworthy that this feature cannot be implemented in standard two-terminal piezoresistive devices, in which sensitivity is intrinsically related to their geometry and materials employed for their fabrication. To demonstrate this feature, the readout experiment was repeated by fixing the stimulation pattern (monophasic voltage pulses with an amplitude of 30 V, duration of 2 ms and frequency of 1 Hz) and changing the biasing condition of the sensor. In particular, the V_{DS} was fixed to –5 V to keep the sensor in its saturation regime, while the V_{GS} was varied from 0 to –3 V with –1 V steps, to progressively move the sensor from the subthreshold regime to the full conductive state. Results are reported in **Figure 4**, in which the output voltage of the front end is reported together with the force

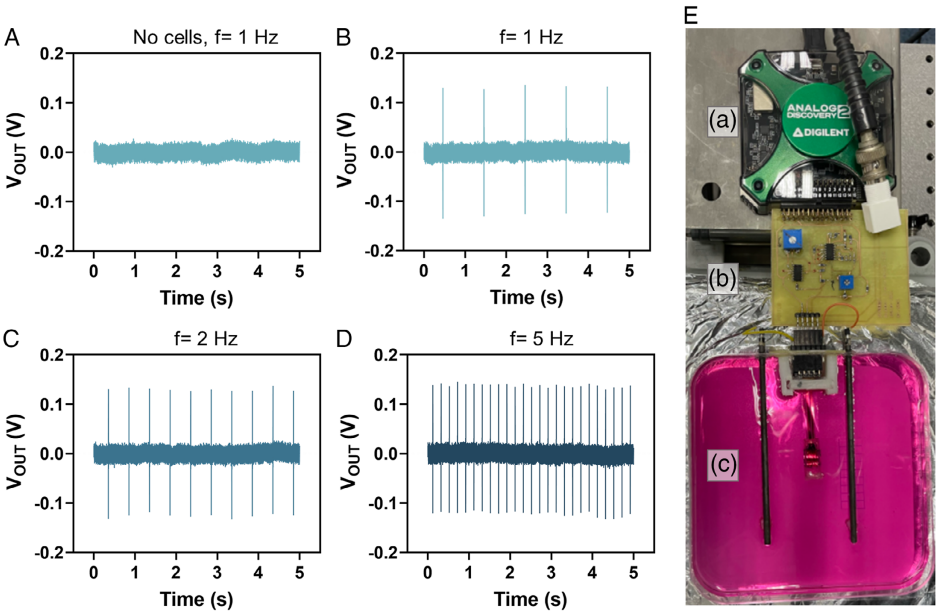

Figure 3. Sensor readout at different measurement conditions: A) application of stimulation (30 V pulses, frequency 1 Hz, duty cycle 2%) on a sensor before muscle tissue integration, B–D) application of stimulation (30 V, duty cycle 2%) on the same sensor after muscle tissue integration, at different frequency values (1, 2, and 5 Hz, respectively). E) Detail of measurement platform showing a) the system employed for interfacing the readout electronics and the PC, b) the custom readout electronics, and c) the cell with carbon electrodes for cell stimulation.

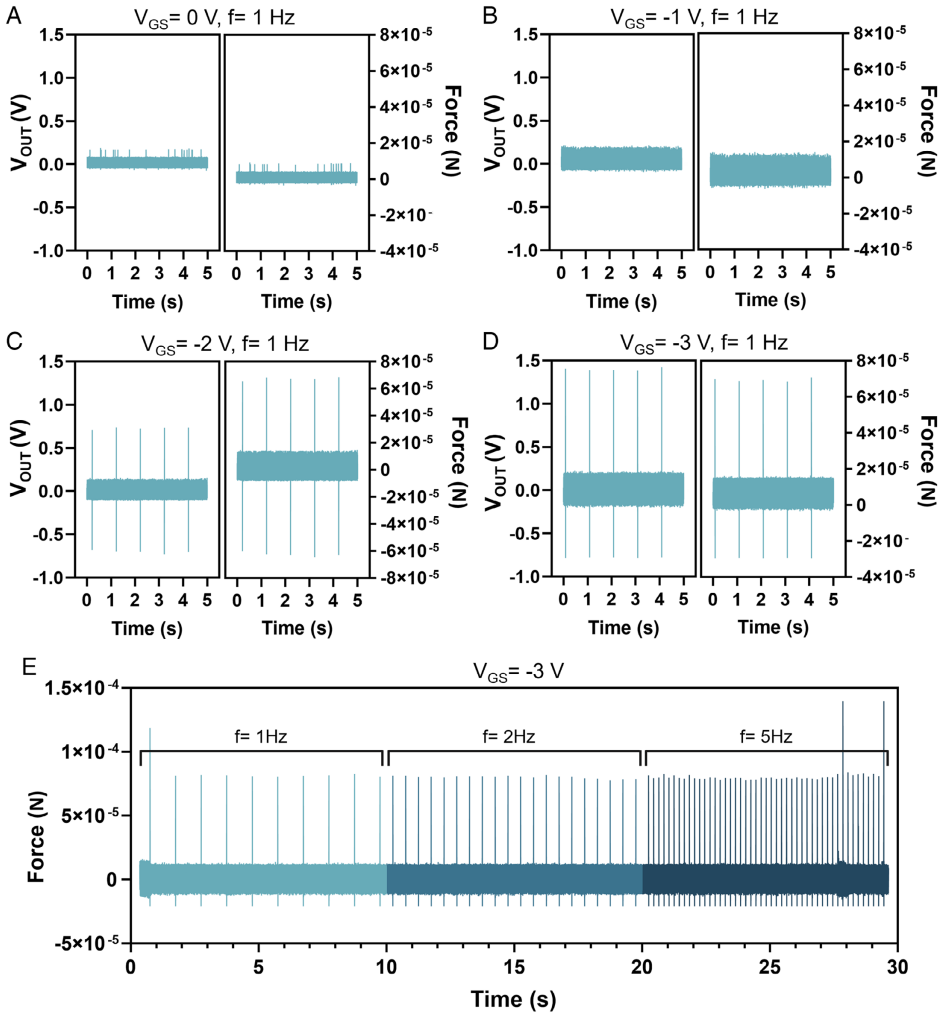

Figure 4. Sensing modulation of the device. A–D) Sensor readout and corresponding force recorded on a sensor during cell stimulation (pulse amplitude 30 V, frequency 1 Hz, duty cycle 2%), for different values of V_{GS} (0, −1, −2, and −3 V, respectively) and fixed $V_{DS} = -5$ V, showing the possibility of the platform to modify sensitivity and improving signal-to-noise ratio for a given force imposed by muscle tissue. E) Force recorded in a 30 s long experiment, by modulating frequency (1, 2, and 5 Hz).

applied by the muscle tissue. The latter value was extrapolated from V_{OUT} knowing the transfer function of the readout electronics and the sensitivity values extrapolated by sensor calibration at different V_{GS} values. Calibration plots for the reported sensor are provided in Supporting Information (Figure S4), along with a detailed explanation about force extraction from output voltage of the front end.

When the device is in the subthreshold regime ($V_{GS} = 0$ V, Figure 4A), only noise was recorded even if cells correctly contracted during the stimulation. By slightly decreasing V_{GS} to –1 V to move the sensor to a more conductive condition (Figure 3Eb), the amplitude of the noise band increased, but no signal was transduced. This result is compatible with the fact that sensitivity values obtained for this sensor at $V_{GS} = 0$ V and $V_{GS} = -1$ V are comparable: therefore, even if the sensors slightly entered into their conductive state, this is not sufficient to ensure signal transduction. When the device is more effectively switched on ($V_{GS} = -2$ V, Figure 4C), sensitivity becomes sufficient to allow detection of tissue contraction. The force extrapolated from V_{OUT} is of about 80 μN, compatible with force values previously reported in similar bioactuators where post deflection systems and video post-processing were used to evaluate the force output, demonstrating the reliability of our strain sensor as a real-time force measurement platform.[22] Interestingly, a further decrease of the V_{GS} value ($V_{GS} = -3$ V, Figure 4D) results in a larger voltage signal, since transistor current increased and so charge carrier mobility does. Nonetheless, when the force is extracted by means of the calibrated sensitivity, the value obtained is substantially identical to the one obtained in the previous condition. Therefore, not only is the capability of the sensor to be tuned to a given force range demonstrated, but also the possibility of improving the signal-to-noise ratio of the voltage signal is exhibited by the system. Indeed, thanks to the larger current flowing in the transistor, a larger output voltage is obtained, while the noise band amplitude increases less because of the band-pass readout function. In Figure 4E, a 30 s long acquisition of cell contraction

is reported, showing the real-time display of the force and the capability of the sensor to follow modification of the stimulation pattern in terms of repetition frequency. More testing is reported in Figure S5, Supporting Information.

2.4. Force Sensing during Drug-Assisted Modulation of Cell Contraction

To prove the potentialities of the proposed approach, the real-time monitoring of muscle cells activity during exposure to chemicals capable of interfering with their contractility was carried out.

The results of such testing are reported in **Figure 5**. Figure 5A shows the effect of raising the concentration of caffeine in the measurement environment, which is known to be a stimulant that enhances muscle contraction by promoting the release of Ca^{2+} ions from the sarcoplasmic reticulum to the cytoplasm.[23] Average force amplitude evaluated in a 10 s recording at different concentrations (from 1 nM to 10 mM, 1 point per decade) is reported with some representative real-time measurement. Stimulation conditions were fixed (monophasic voltage pulse with an amplitude of 30 V, a duration of 2 ms, and a repetition frequency of 1 Hz), as well as sensor bias ($V_{DS} = -5$ V, $V_{GS} = -1$ V). V_{GS} selection was determined by the previously recorded maximum (see calibration curves reported in Figure S6, Supporting Information) and that required to sufficiently identify contractions over the noise band. In this way, a larger dynamic range for evaluating force increase was enabled. The reported results show that forces were progressively altered with caffeine concentration: a significant increase was recorded from the lowest concentration employed (1 nM), while a substantial plateau was obtained at 1 μM. From this concentration onward, error bars (1–σ standard deviation) became broader, due to the significant increase of spontaneous contraction events that are sometimes characterized by a force significantly larger than the one of evoked contractions, as depicted by the measurement recorded at the maximum concentration of 10 mM. The complete set of plots of this experiment and videos of the contracting bioactuator at 0 and 10 mM of caffeine are reported in Supporting Information (Figure S7 and Movie S2, respectively).

Figure 5b shows the results obtained at a fixed concentration of dantrolene, which, contrary to caffeine, is a relaxant that blocks the calcium release and therefore reduces contraction force.[24] In this experiment, a concentration of 100 μM of dantrolene was used in the measurement environment; stimulation with monophasic pulses (amplitude 30 V, duration 2 ms, repetition frequency 1 Hz) was also imposed throughout the experiment. The sensor was biased with $V_{DS} = -5$ V and $V_{GS} = -3$ V to let it operate at maximum sensitivity (see calibration plot in Figure S8, Supporting Information), thus ensuring the largest dynamic range toward the expected force reduction. The sensor readout was carried out by applying the stimulation for 10 s at different times after the addition of dantrolene (5, 20, 30, 40, 50, and 60 min) to avoid force reduction due to cell fatigue from prolonged stimulation. Average and 1–σ error bars over the 10 s recording were evaluated. It is possible to observe that, with respect to the acquisition carried out immediately before the application of dantrolene ($t = 0$ min), the force substantially

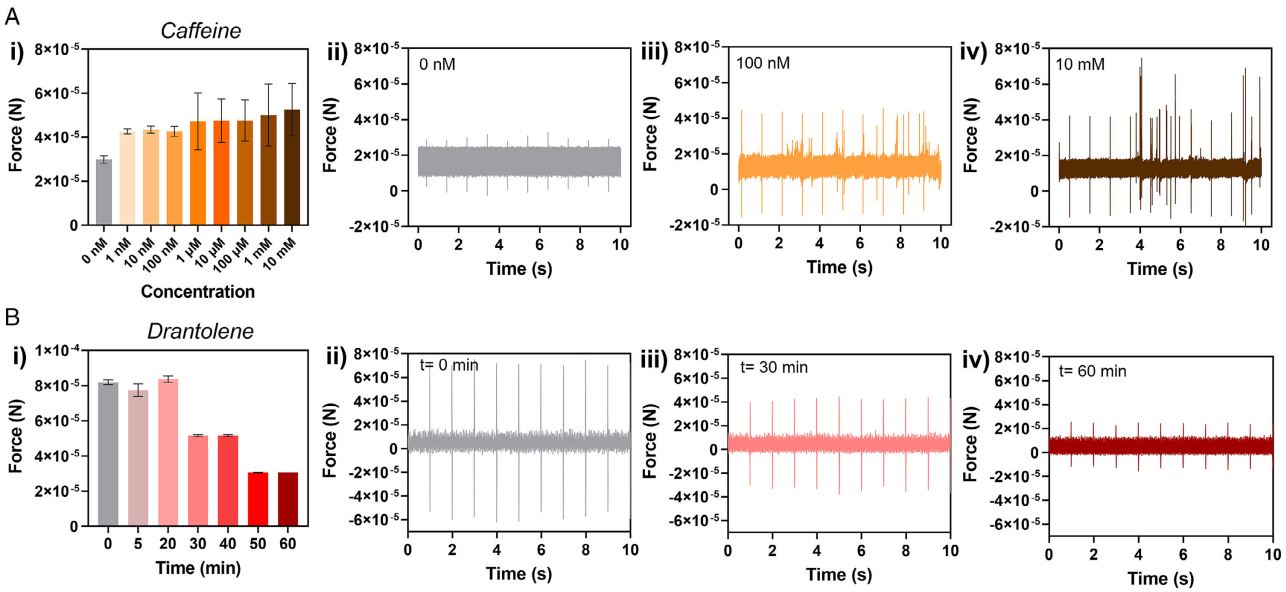

Figure 5. Evaluation of the effects of caffeine (stimulant drug) and dantrolene (relaxant drug) on contraction force. A) Sensor response to different concentration of caffeine in the measurement environment, at a fixed cell stimulation (pulse amplitude 30 V, frequency 1 Hz, duty cycle 2%) and fixed sensor bias ($V_{DS} = -5$ V, $V_{GS} = -2$ V). From left to right: average response calculated on peaks acquired in a 10 s long measurement at different concentrations of caffeine, and examples of real-time plot for 0 nM, 100 nM, and 10 mM caffeine concentration. In the latter, spontaneous contractions were also recorded. B) Evolution of the force applied by the muscle tissue in time after the addition of a given concentration of dantrolene in the measurement environment for a fixed electrical stimulation (pulse amplitude 30 V, frequency 1 Hz, duty cycle 2%) and sensor bias ($V_{DS} = -5$ V, $V_{GS} = -3$ V). From left to right: average force calculated on a period of 10 s of cell recordings, and examples of force decreases at different time (before dantrolene introduction in the measurement environment, after 30 min and after 60 min).

halved within the first 30 min, and another 50% reduction was noticed after 50 min. This is also clearly displayed by selected plots recorded at $t = 0$ min, $t = 30$ min, and $t = 60$ min; all recorded timepoints and videos of the contracting bioactuator at $t = 0$ min and $t = 60$ min are reported in Supporting Information (Figure S9 and Movie S3, respectively). Therefore, the average force decreased from the initial 80 μN to around 20 μN by the end of experiment.

3. Conclusion

In this work, we demonstrated a novel approach for real-time monitoring of the force exerted by muscle bioactuators by means of organic transistor-based strain sensors. The employment of electronic sensors allows the recording of contraction events of electrically stimulated 3D-bioengineered muscle tissues, providing a direct transduction into electrical signals that can be acquired by digital units for real-time visualization and further data elaboration. Moreover, programmable sensitivity to deformation is enabled by the employment of a transistor instead of a conventional piezoresistive device. Several sensors have been calibrated in a low-force range, and their performances have been fully demonstrated: in particular, the absence of significant cross talk between stimulation signals and recorded force was verified, as well as the capability of sensing performance modulation through sensor bias alteration. Finally, the real-time contraction force monitoring of muscles treated with stimulant and relaxant drugs, caffeine and dantrolene, respectively, was successfully tested demonstrating the potential of our technology as a drug testing platform. These results demonstrate the suitability of organic electronic devices for the development of next generation sensing platforms for different applications, beyond soft robotics and toward a more general exploitation in the various fields of bioengineering such as the development of in vitro muscle models and drug testing.

4. Experimental Section

Device Fabrication: Strain sensors were fabricated on commercial, 13 μm thick polyethylene terephthalate foils (Goodfellow). A bottom gate-bottom contact OFET structure was employed: the first transistor element implemented was the gate, obtained by a standard photolithographic process of a thermally evaporated aluminum layer (100 nm thick). To ensure low voltage operation of fabricated devices, a double-layer hybrid dielectric was employed as gate insulator.[25] Aluminum surface was first oxidized by annealing in oven at 50 °C overnight, and then a 200 nm thick layer of Parylene C (Specialty Coating Systems) was deposited by chemical vapor deposition, using an adhesion promoter (Sylane A 174) to enhance the film quality. Source and drain contact were made in thermally evaporated gold (60 nm thick), patterned in an interdigitated structure by photolithography. The aspect ratio of the device (ratio between channel width, W, and channel length, L) is $W/L = 2300$. The 6,13-bis(triisopropylsilylethynyl)pentacene (TIPS pentacene, Sigma-Aldrich) was chosen as organic semiconductor: the active layer of the transistor was obtained by drop-casting a 1 wt% solution of TIPS pentacene in anhydrous anisole (Sigma-Aldrich) onto the channel area. The film was formed by letting the solution dry at room temperature in a fume hood. To prevent the degradation of the organic semiconductor during operation in liquid, and to ensure an overall biocompatibility of the sensor,[26] a 2 μm thick layer of Parylene C was deposited as encapsulant. The notches used to assemble the 3D-bioengineered muscle tissue on the strain sensor were designed in AutoCAD and then processed with Slic3r and Cellink Heartware software to obtain the gcode for the Cellink's Inkredible+ 3D bioprinter. PDMS at a 20:1 ratio was used for 3D printing of the notches, and they were cross-linked at 65 °C overnight.

Electrical and Electromechanical Characterization: Sensors' preliminary electrical characterization was carried out using a Keithley 2636 SourceMeter provided with a custom MATLAB graphic user interface. The same system was used during sensor calibration with forces, combined with a mechanical indenter connected with a dynamometer (Imada Digital Force Measurement Gauge). A 3D-printed, acrylonitrile butadiene styrene (BASF) frame was fabricated to support the sensor and allow the application of a reproducible deformation for the different forces applied by the indenter.

Sensor Readout: The acquisition of sensors' signals during experiments was ensured by a custom-made analog front end, designed to be integrated with an Analog Discovery 2 (Digilent) Oscilloscope and Logic Analyzer. Details about the functional blocks of the readout electronics are reported in Supporting Information. The software Waveforms was used for data real-time visualization and saving.

C2C12 Cell Culture and Fabrication of the 3D Skeletal Muscle Tissue: C2C12 mouse myoblasts were purchased from ATCC and cultured in T-175 flasks using growth media (GM) composed of high-glucose Dulbecco's modified Eagle's medium (DMEM), supplemented with 10% fetal bovine serum, 200 nM l-glutamine, and 1% penicillin-streptomycin (all from Gibco). Once cells reached the 80% of confluency, they were trypsinized and mixed with a hydrogel made of 30% v/v Matrigel, 4 U mL^{-1} of thrombin, 4 mg mL^{-1} of fibrinogen, and 16% v/v of GM supplemented with 1 mg ml^{-1} aminocaproic acid (ACA, Sigma-Aldrich) at a concentration of 10 million mL^{-1} C2C12 cells. Then, this cell-laden hydrogel was mold casted in a PDMS-based (ratio 20:1) circular rings (1.3 and 1.6 cm diameter for internal and external rings, respectively) that were previously 3D printed with the Cellink's Inkredible+ 3D bioprinter and cured at 65 °C overnight. The cell-laden hydrogel was cultured in the mold for 2 days in GM + ACA in an incubator at 37 °C and 5% CO_2, then transferred to a petri dish containing two notches (same design as the ones printed on top of the strain sensor) where the tissue was assembled and cultured in differentiation media (DM) composed of DMEM supplemented with 10% horse serum (Gibco), 200 nM l-glutamine, 1% penicillin–streptomycin, insulin-like growth factor (IGF)-1 (50 ng ml^{-1}; Sigma-Aldrich), and 1 mg ml^{-1} of ACA. Muscle tissues were left to differentiate for at least 7 days before performing experiments.

Assembly of the 3D-Bioengineered Skeletal Muscle Tissue into the Strain Sensor: To conduct the real-time force measurement experiments, the 3D-bioengineered skeletal muscle ring was carefully removed from culture petri dish using sterilized tweezers and assembled in the notches located on top of the flexible strain sensor. This process was performed in a square petri dish (refer to the detailed measurement set up in Figure 3E) containing warm DM to minimize any stress on the bioengineered muscle during handling.

Chemical Modulation of Contraction Force: Caffeine (Sigma-Aldrich) and dantrolene sodium (Sigma-Aldrich) were used to stimulate contraction force and relaxation of the muscle tissue, respectively, following the protocol reported by Zhao et al.[16] Caffeine was dissolved in phosphate buffer saline (PBS) in series of different dilutions, which were added to the cell media every 1 min increasing the concentrations from 1 nM to 10 mM (all concentrations are shown in Figure S6, Supporting Information). Muscle tissues were electrically stimulated (30 V, 2 ms, 1 Hz) during the entire timeline of the experiment and real-time measurements were recorded for 10 s before adding the next caffeine concentration. For the treatment with dantrolene sodium, a fixed final concentration of 100 μM was used. Dantrolene was first dissolved in dimethyl sulfoxide (Sigma-Aldrich) and then diluted at a ratio of 1:4 with PBS. The sensor readout was carried out by applying the stimulation for 10 s at different times after the addition of dantrolene (5, 20, 30, 40, 50, and 60 min).

Supporting Information

Supporting Information is available from the Wiley Online Library or from the author.

Acknowledgements

J.F., S.L., G.C., P.C., and S.S. acknowledge the financial support from the European Union's Horizon Europe research and innovation program under grant agreement no. 101070328 (Biomeld). M.G. acknowledges the financial support from the Spanish Ministry of Science through the Ramon y Cajal grant no. RYC2020-945030119-I and "Unidad Maria de Maetzu" funded by Agencia Estatal de Investigación (2021; grant no. CEX2021-001202-M). S.S., M.G., and J.F. acknowledge CERCA program by the Generalitat de Catalunya, the Secretaria d'Universitats i Recerca del Departament d'Empresa i Coneixement de la Generalitat de Catalunya through the project 2021 SGR 01606, and the "Centro de Excelencia Severo Ochoa", funded by Agencia Estatal de Investigación (grant no. CEX2018-000789-S).

Conflict of Interest

The authors declare no conflict of interest.

Author Contributions

Stefano Lai: Conceptualization (lead); Data Curation (lead); Formal Analysis (lead); Funding Acquisition (lead); Investigation (lead); Methodology (lead); Project Administration (lead); Resources (lead); Software (lead); Supervision (lead); Validation (lead); Visualization (lead); Writing—Original Draft (lead); and Writing—Review and Editing (lead). **Judith Fuentes**: Data Curation (equal); Formal Analysis (equal); Investigation (lead); Methodology (lead); Visualization (equal); Writing—Original Draft (equal); and Writing—Review and Editing (equal). **Maria Guix**: Conceptualization (lead); Data Curation (equal); Formal Analysis (lead); Investigation (lead); Methodology (lead); Project Administration (lead); Resources (lead); Software (equal); Supervision (lead); Validation (lead); Visualization (lead); Writing—Original Draft (lead); and Writing—Review and Editing (lead). **Giulia Casula**: Formal Analysis (supporting); Investigation (equal); and Writing—Original Draft (supporting). **Piero Cosseddu**: Conceptualization (supporting); Supervision (supporting); and Writing—Original Draft (supporting). **Samuel Sánchez**: Conceptualization (lead); Funding Acquisition (lead); Project Administration (equal); Resources (lead); Supervision (lead); Validation (lead); and Writing—Review and Editing (equal). **Stefano Lai** and **Judith Fuentes** contributed equally to this work.

Data Availability Statement

The data that support the findings of this study are available from the corresponding author upon reasonable request.

Keywords

bioengineerings, flexible electronics, muscle-based actuators, organic field-effect transistors, soft robotics

Received: May 22, 2024
Revised: September 17, 2024
Published online: October 14, 2024

[1] M. Guix, C. C. Mayorga-Martinez, A. Merkoçi, *Chem. Rev.* **2014**, *114*, 6285.
[2] F. Soto, J. Wang, R. Ahmed, U. Demirci, *Adv. Sci.* **2020**, *7*, 2002203.
[3] V. A. Webster-Wood, M. Guix, N. W. Xu, B. Behkam, H. Sato, D. Sarkar, S. Sanchez, M. Shimizu, K. K. Parker, *Bioinspir. Biomim.* **2023**, *18*, 015001.
[4] C. Appiah, C. Arndt, K. Siemsen, A. Heitmann, A. Staubitz, C. Selhuber-Unkel, *Adv. Mater.* **2019**, *31*, 1807747.
[5] J. Jiang, Z. Yang, A. Ferreira, L. Zhang, *Adv. Intell. Syst.* **2022**, *4*, 2100279.
[6] S.-J. Park, M. Gazzola, K. S. Park, S. Park, V. Di Santo, E. L. Blevins, J. U. Lind, P. H. Campbell, S. Dauth, A. K. Capulli, F. S. Pasqualini, S. Ahn, A. Cho, H. Yuan, B. M. Maoz, R. Vijaykumar, J.-W. Choi, K. Deisseroth, G. V. Lauder, L. Mahadevan, K. K. Parker, *Science* **2016**, *353*, 158.
[7] K. Y. Lee, S.-J. Park, D. G. Matthews, S. L. Kim, C. A. Marquez, J. F. Zimmerman, H. A. M. Ardoña, A. G. Kleber, G. V. Lauder, K. K. Parker, *Science* **2022**, *375*, 639.
[8] R. Raman, C. Cvetkovic, S. G. M. Uzel, R. J. Platt, P. Sengupta, R. D. Kamm, R. Bashir, *Proc. Natl. Acad. Sci. U.S.A.* **2016**, *113*, 3497.
[9] Y. Kim, Y. Yang, X. Zhang, Z. Li, A. Vázquez-Guardado, I. Park, J. Wang, A. I. Efimov, Z. Dou, Y. Wang, J. Park, H. Luan, X. Ni, Y. S. Kim, J. Baek, J. J. Park, Z. Xie, H. Zhao, M. Gazzola, J. A. Rogers, R. Bashir, *Sci. Robot.* **2023**, *8*, eadd1053.
[10] T. Bruegmann, T. van Bremen, C. C. Vogt, T. Send, B. K. Fleischmann, P. Sasse, *Nat. Commun.* **2015**, *6*, 7153.
[11] R. Kinjo, Y. Morimoto, B. Jo, S. Takeuchi, *Matter* **2024**, *7*, 948.
[12] C. Vesga-Castro, J. Aldazabal, A. Vallejo-Illarramendi, J. Paredes, *eLife* **2022**, *11*, e77204.
[13] M. Rausch, D. Böhringer, M. Steinmann, D. W. Schubert, S. Schrüfer, C. Mark, B. Fabry, *Biophys. J.* **2020**, *118*, 657.
[14] A. Iuliano, M. Haalstra, R. Raghuraman, K. Bielawski, A. P. Bholasing, E. van der Wal, J. C. de Greef, W. W. M. P. Pijnappel, *Adv. Mater. Technol.* **2023**, *8*, 2300845.
[15] A. S. Smith, S. M. Luttrell, J.-B. Dupont, K. Gray, D. Lih, J. W. Fleming, N. J. Cunningham, S. Jepson, J. Hesson, J. Mathieu, L. Maves, B. J. Berry, E. C. Fisher, N. J. Sniadecki, N. A. Geisse, D. L. Mack, *J. Tissue Eng.* **2022**, *13*, 1.
[16] H. Zhao, Y. Kim, H. Wang, X. Ning, C. Xu, J. Suh, M. Han, G. J. Pagan-Diaz, W. Lu, H. Li, W. Bai, O. Aydin, Y. Park, J. Wang, Y. Yao, Y. He, M. T. A. Saif, Y. Huang, R. Bashir, J. A. Rogers, *Proc. Natl. Acad. Sci. U.S.A.* **2021**, *118*, e2100077118.
[17] K. Feron, R. Lim, C. Sherwood, A. Keynes, A. Brichta, P. C. Dastoor, *Int. J. Mol. Sci.* **2018**, *19*, 2382.
[18] M. Bolognesi, M. Prosa, M. Seri, in *Sustainable Strategies in Organic Electronics*, Elsevier, Amsterdam **2022**, pp. 297–338.
[19] P. Cosseddu, S. Milita, A. Bonfiglio, *IEEE Electron. Device Lett.* **2012**, *33*, 113.
[20] V. Scenev, P. Cosseddu, A. Bonfiglio, I. Salzmann, N. Severin, M. Oehzelt, N. Koch, J. P. Rabe, *Org. Electron.* **2013**, *14*, 1323.
[21] T. Cramer, L. Travaglini, S. Lai, L. Patruno, S. de Miranda, A. Bonfiglio, P. Cosseddu, B. Fraboni, *Sci. Rep.* **2016**, *6*, 38203.
[22] M. Guix, R. Mestre, T. Patiño, M. de Corato, J. Fuentes, G. Zarpellon, S. Sánchez, *Sci. Robot.* **2021**, *6*, 1.
[23] A. Fukutani, S. Kunimatsu, T. Isaka, *Sci. Rep.* **2022**, *12*, 7980.
[24] T. Krause, M. U. Gerbershagen, M. Fiege, R. Weißhorn, F. Wappler, *Anaesthesia* **2004**, *59*, 364.
[25] P. Cosseddu, S. Lai, M. Barbaro, A. Bonfiglio, *Appl. Phys. Lett.* **2012**, *100*, 093305.
[26] M. Golda-Cepa, K. Engvall, M. Hakkarainen, A. Kotarba, *Prog. Org. Coat.* **2020**, *140*, 105493.